Inorganic Chemistry

Article

pubs.acs.org/IC

Explorations of New Second-Order Nonlinear Optical Materials in the Ternary Rubidium Iodate System: Noncentrosymmetric β-$RbIO_3(HIO_3)_2$ and Centrosymmetric $Rb_3(IO_3)_3(I_2O_5)(HIO_3)_4(H_2O)$

Xiang Xu, Bing-Ping Yang, Chao Huang, and Jiang-Gao Mao*

State Key Laboratory of Structural Chemistry, Fujian Institute of Research on the Structure of Matter, Chinese Academy of Sciences, Fuzhou 350002, People's Republic of China

Supporting Information

ABSTRACT: Two new rubidium iodates, namely, β-$RbIO_3(HIO_3)_2$ (**1**, $P1$) and $Rb_3(IO_3)_3(I_2O_5)(HIO_3)_4(H_2O)$ (**2**, $P2_1/c$), have been synthesized by hydrothermal reaction and their structures determined by single-crystal X-ray diffraction. Compound **1** exhibits IO_3^- anions and neutral HIO_3 molecules which are interconnected by Rb^+ cations into three-dimensional structure. Compound **2** features a two-dimensional layered structure formed by IO_3^- anions and neutral HIO_3 and dimeric I_2O_5 molecules interconnected by Rb^+ cations. Large bulk crystal of **1** with dimensions of several millimeters has been grown. UV−vis−NIR transmission spectroscopy measurements on a slab of a polished crystal of **1** indicated that the crystal possesses a short-wavelength absorption edge onset at 305 nm. Powder second-harmonic generation (SHG) measurements on sieved crystals revealed that **1** is a type I phase-matchable material with an SHG response about 1.5 times that of KH_2PO_4. The Vickers hardness of crystal of **1** has been measured to be 110 HV, and the laser-induced damage threshold has been confirmed to be 18.26 J/cm^2 with a laser wavelength of 1064 nm and a pulse duration of 10 ns. Moreover, thermal stabilities and vibrational spectra for both **1** and **2** have also been studied.

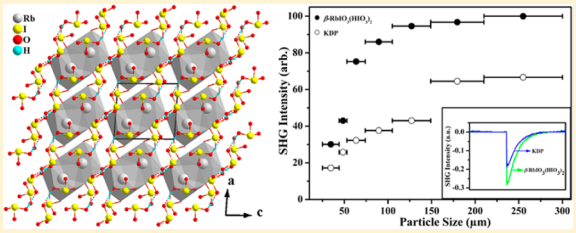

INTRODUCTION

Inorganic second-order nonlinear optical (NLO) materials have attracted considerable research interest due to their important applications in photonic technologies.[1−5] Metal iodates can exhibit excellent second-order NLO properties due to the asymmetric coordination polyhedron of the I^{5+} cation, which is caused by the second-order Jahn−Teller (SOJT) distortion.[6−15] Simple ternary metal iodates, such as α-$LiIO_3$, have been widely studied as second-order NLO materials in the past century.[16] During the past decade, the combination of transition-metal ions with d^0 electronic configurations (Ti^{4+}, Nb^{5+}, V^{5+}, and Mo^{6+}, etc.) or cations containing lone-pair electrons such as Pb^{2+} and Bi^{3+} with IO_3^- anions has been found to be an effective synthetic route for designing new noncentrosymmetric (NCS) iodates with better NLO properties by the constructive addition of polarization from both types of asymmetric building units,[17−24] which led to the discovery of a large number of new second-harmonic generation (SHG) materials, including $AMoO_3(IO_3)$ (A = Li, Rb, Cs),[17a,21c] $A_2Ti(IO_3)_6$ (A = Li, Na),[18a,b] $BaNbO(IO_3)_5$,[20a] $A(VO)_2(IO_3)_3O_2$ (A = K, Rb, Cs, NH_4),[17b,20b] $NaVO_2(IO_3)_2(H_2O)$,[20c] $BiO(IO_3)$,[22] $Bi_2(IO_4)(IO_3)_3$,[23] and $PbPt(IO_3)_6(H_2O)$.[24b] Recently it has been reported that the introduction of transition-metal ions with a square-planar AO_4 geometry (A = Pd^{2+} or Au^{3+}) into iodates can also form NCS structures with good SHG properties;[25] for example, $BaPb(IO_3)_4$[25a] and $RbAu(IO_3)_4$[25b] exhibit SHG efficiency about 0.4 and 1.3 times that of $KTiOPO_4$ (KTP), respectively.

Previous studies on iodates also revealed that reaction conditions such as temperature, pH values of the reaction media, and molar ratios of the reactants have a great influence on the compositions, structures, and SHG properties of the materials formed. For example, through adjustment of the synthetic conditions, four potassium vanadyl iodates in the K−V−I−O quaternary system, namely, α-$KVO_2(IO_3)_2(H_2O)$, β-$KVO_2(IO_3)_2(H_2O)$, $K_4[(VO)(IO_3)_5]_2(HIO_3)(H_2O)_2{\cdot}H_2O$, and $K(VO)_2O_2(IO_3)_3$, have been isolated.[20b] For the ternary alkali-metal iodate system, several new compounds have been obtained under different synthetic conditions,[8,9,11] among which NaI_3O_8[9] and α-$Cs_2I_4O_{11}$[8] exhibit strong SHG responses. Hence, we focus our efforts on the ternary rubidium iodate system. We deem that new ternary phases can be found by careful selection of the conditions for the hydrothermal reactions. So far, several compounds in the rubidium iodate system have been reported. As for the ternary rubidium iodate system, $RbIO_3$[26a] crystallizes in the acentric space group $R3m$, whereas both α-$RbIO_3(HIO_3)_2$[26b] and $Rb_2(I_3O_8)(IO_3)(HIO_3)_2(H_2O)$[26c,d] crystallize in the centric space group $P\bar{1}$. Although $RbIO_3$ exhibits an acentric structure, its NLO property has not been studied so far. $RbIO_3$ contains only IO_3^- anions, whereas α-$RbIO_3(HIO_3)_2$ is composed of both IO_3^- anions and neutral HIO_3 molecules. $Rb_2(I_3O_8)(IO_3)(HIO_3)_2(H_2O)$ is more complex, and its structure contains

Received: November 21, 2013
Published: January 15, 2014

   dx.doi.org/10.1021/ic4028942 | Inorg. Chem. 2014, 53, 1756−1763

IO_3^-, polymeric $I_3O_8^-$, and neutral HIO_3. All these anions or molecules are bridged by Rb^+ cations into three-dimensional (3D) structures in these three compounds. The introduction of transition-metal ions with d^0 electronic configurations into the rubidium iodates afforded many types of novel anionic structures, including zero-dimensional (0D) $[Zr(IO_3)_6]^{2-}$ in $Rb_2Zr(IO_3)_6$[28] and $[Ti(IO_3)_6]^{2-}$ in $Rb_2Ti(IO_3)_6$,[18b] one-dimensional (1D) $[VO_2(IO_3)_2]_n^{n-}$ in $RbVO_2(IO_3)_2$,[17b] 1D $[(VO)_2(IO_3)_3O_2]_n^{n-}$ in $Rb(VO)_2(IO_3)_3O_2$,[17b] 1D $[UO_2(CrO_4)(IO_3)_2]_n^{2n-}$ in $Rb_2UO_2(CrO_4)(IO_3)_2$,[27] 1D $[UO_2(CrO_4)(IO_3)(H_2O)]_n^{n-}$ in $RbUO_2(CrO_4(IO_3)(H_2O)$,[27] and three-dimensional (3D) $[MoO_3(IO_3)]^-$ in $RbMoO_3(IO_3)$.[17a] It is demonstrated that these iodates show great structural variability. Our research efforts on the systematic explorations of new ternary rubidium iodates led to the discovery of two new rubidium iodates, namely, noncentrosymmetric β-$RbIO_3(HIO_3)_2$ (**1**) and centrosymmetric $Rb_3(IO_3)_3(I_2O_5)(HIO_3)_4(H_2O)$ (**2**). Herein, we report the syntheses, crystal structures, thermal stabilities, and infrared spectra for both compounds. The hardness, laser-induced damage threshold, UV–vis–NIR transmission spectrum, and second-order NLO properties for **1** were also measured.

EXPERIMENTAL SECTION

Reagents and Instrumentation. All of the chemicals were analytically pure from commercial sources and were used without further purification. Rb_2CO_3 (99.9%) and I_2O_5 (99.0%) were purchased from Sinopharm Chemical Reagent Co. Ltd.

Powder X-ray diffraction (XRD) patterns of ground crystals were collected on a Rigaku MiniFlex II diffractometer using monochromated Cu Kα radiation (λ = 1.540598 Å) at room temperature with a step size of 0.02°.

Infrared (IR) spectra were recorded on a Nicolet AVATAR 370 FT-IR infrared spectrophotometer as KBr pellets in the range of 4000–400 cm^{-1}.

Microprobe elemental analyses were performed on a field emission scanning electron microscope (JSM6700F) equipped with an energy-dispersive X-ray spectroscope (Oxford INCA).

Thermogravimetric analyses (TGA) and differential scanning calorimetry (DSC) were carried out with a NETZCH STA 449F3 unit at a heating rate of 10 °C/min under a N_2 atmosphere.

The hardness measurements of crystals of **1** were performed on a 401 MVA micro-Vickers hardness tester.

The solid-state circular dichroism (CD) spectra were measured on an MOS-450 spectropolarimeter using a 1.1 mm thick slab of a crystal of **1**.

The UV–vis–NIR transmittance spectrum of a crystal of **1** and the UV–vis–NIR optical diffuse reflectance spectrum of **2** were recorded at room temperature on a PerkinElmer Lambda 950 spectrophotometer. A 1.5 mm thick slab of **1** which was polished on both sides was used for the transmittance spectrum measurement (Figure 1c). Colorless crystals of **2** were ground for the optical diffuse reflectance spectrum measurement, and a $BaSO_4$ plate was used as a standard (100% reflectance).

The laser-induced damage threshold of **1** was determined using a Q-switched Nd:YAG laser operating in TEM_{00} mode at a wavelength of 1064 nm with pulse duration τ = 10 ns. Slabs of crystals of **1** with the surface polished were positioned on the plane perpendicular to the laser beam. The energy of the laser radiation was gradually increased until the crystal was damaged, and a power meter records the energy density of the input laser beam of a single pulse. The criterion for laser damage was that a spark was observed at the crystal breakdown.

The measurements of the powder frequency-doubling effects for **1** were carried out on the sieved samples by means of the modified method of Kurtz and Perry.[29] Radiation (1064 nm) generated by a Q-switched Nd:YAG solid-state laser was used as the fundamental frequency light. Crystals of **1** were ground and sieved into several distinct particle size ranges (25–45, 45–53, 53–75, 75–105, 105–150, 150–210, and 210–300 μm). Sieved KH_2PO_4 (KDP) samples with the same size ranges were used as references. The ratio of the SHG effect of **1** to that of KDP was calculated on the basis of the density of second-harmonic outputs of **1** and KDP with the same particle size range of 150–210 μm. Furthermore, since it is commonly reported that the SHG response of BBO is 5.6 times that of KDP, a β-BaB_2O_4 sample with a particle size of 150–210 μm was also selected as a standard sample for measurement system adjustment and to ensure accurate measurement of the ratio of the SHG coefficient of **1** to that of KDP.

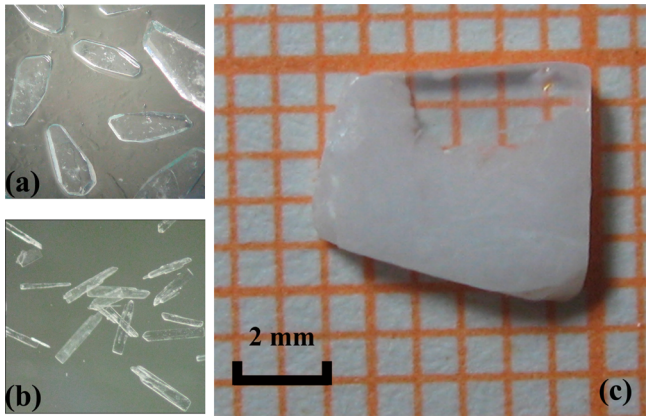

Figure 1. As-grown small crystals of **1** (a) and **2** (b) and a 1.5 mm thick polished slab of **1** used for transmittance spectral measurement (c).

Synthesis. Both compounds **1** and **2** were synthesized by hydrothermal reactions of a mixture of Rb_2CO_3 and I_2O_5 in water sealed in an autoclave equipped with a Teflon liner (25 mL). The loaded compositions were Rb_2CO_3 (230.9 mg, 1.0 mmol), I_2O_5 (1335.2 mg, 4 mmol), and H_2O (4 mL) for **1** and Rb_2CO_3 (57.7 mg, 0.25 mmol), I_2O_5 (667.6 mg, 2 mmol), and H_2O (2 mL) for **2**. The mixture was heated at 230 °C for 20 h, followed by slow cooling to ambient temperature at a rate of 1.0 °C/h. The final pH values of the reaction media were less than 1.0. The reaction products were washed with ethanol and then dried in air. These crystals are easily dissolved in water; hence, water could not be used to wash the crystals. Colorless block-shaped crystals of **1** and plate-shaped crystals of **2** were obtained as single phases in yields of about 88% and 92% (based on Rb_2CO_3), respectively (Figure 1a,b). The purities of these single phases were confirmed by powder XRD studies (Figure S1, Supporting Information). The energy-dispersive spectrometry (EDS) elemental analyses on several single crystals for each compound gave average Rb:I molar ratios of 1:2.80 and 1:3.24 for **1** and **2**, respectively, which are in good agreement with those determined from single-crystal X-ray structure analyses.

The growth of large crystals of **1** was performed using the spontaneous nucleation hydrothermal method within a large autoclave. A mixture of Rb_2CO_3 (1732 mg, 7.5 mmol), I_2O_5 (10014.3 mg, 30 mmol), and H_2O (30 mL) was loaded into an autoclave equipped with a Teflon liner (500 mL). The autoclave was then quickly heated to 230 °C, held at that temperature for 50 h, and slowly cooled to ambient temperature at a rate of 0.6 °C/h. Bulk crystals of **1** with a large size of several millimeters were obtained successfully (Figure 1c). Although the large bulk crystals exhibit obvious crystal defects such as white inclusions, there are large tansparent areas with high optical quality which are large enough for some optical property characterizations, such as transmission spectroscopy and laser-induced damage threshold determination.

Single-Crystal Structure Determination. Single-crystal X-ray diffraction data of both compounds were collected on an Agilent Technologies SuperNova dual-wavelength CCD diffractometer with Mo Kα radiation (λ = 0.71073 Å) at 293 K. The data reduction was performed with the program CrysAlisPro, and absorption correction

dx.doi.org/10.1021/ic4028942 | Inorg. Chem. 2014, 53, 1756–1763

based on the multiscan method (for **1**) or Gaussian method (for **2**) was applied.[30] Both structures were solved by direct methods and refined by full-matrix least-squares fitting on F^2 using SHELX-97.[31] The centrosymmetric triclinic space group $P\bar{1}$ was suggested for **1** when the structure was checked for possible missing symmetry elements with PLATON.[32] Structure solution and refinement based on the centrosymmetric space group $P\bar{1}$ can also give an approximately acceptable result (R1 = 0.0480 and wR1 = 0.1108 for $I > 2\sigma(I)$), but it is inconsistent with the SHG response observed for **1**. Thus, we chose the noncentrosymmetric space group $P1$ for structure solution and refinement and obtained better refinements (R1 = 0.0269 and wR1 = 0.0542 for $I > 2\sigma(I)$). The refined Flack parameter of 0.059(14) is close to zero, which is also indicative of the noncentrosymmetric space group $P1$.[33] All non-hydrogen atoms were refined with anisotropic thermal parameters. On the basis of the requirement of charge balance and results of bond valence calculations, O(9), O(12), O(15), and O(18) in **1** and O(17), O(20), O(23), and O(26) in **2** were assigned to hydroxyl groups; their calculated bond valences are −1.34, −1.37, −1.53, −1.47,-1.47, −1.34, −1.38, and −1.38, respectively. All hydrogen atoms except those associated with water molecules in **2** are located at the geometrically calculated positions and refined with isotropic thermal parameters. H(1WA) and H(1WB) in **2** were located from difference Fourier maps and refined with isotropic thermal parameters. Crystallographic data are summarized in Table 1. Selected bond distances are listed in Table 2. More details on the crystallographic studies are given in the Supporting Information.

Table 1. Crystallographic Data for the Two Compounds

	1	2
formula	β-$RbIO_3(HIO_3)_2$	$Rb_3(IO_3)_3(I_2O_5)(HIO_3)_4(H_2O)$
fw	612.19	1836.56
temp, K	293(2)	293(2)
cryst syst	triclinic	monoclinic
space group	$P1$	$P2_1/c$
a, Å	7.4936(4)	8.5195(3)
b, Å	7.5769(3)	25.5012(7)
c, Å	8.2308(4)	13.3874(7)
α, deg	77.881(4)	90
β, deg	84.744(4)	111.053(4)
γ, deg	82.716(4)	90
V, Å^3	452.21(4)	2714.36(19)
Z	2	4
D_{calcd}, g·cm^{-3}	4.496	4.494
μ(Mo Kα), mm^{-1}	15.738	15.731
R_{int}	0.0333	0.0456
GOF on F^2	0.977	1.057
Flack factor	0.059(14)	N/A
R1, wR2 ($I > 2\sigma(I)$)[a]	0.0269, 0.0543	0.0324, 0.0666
R1, wR2 (all data)	0.0294, 0.0559	0.0384, 0.0706

[a] $R1 = \sum||F_o| - |F_c||/\sum|F_o|$. $wR2 = [\sum w(F_o^2 - F_c^2)^2/\sum w(F_o^2)^2]^{1/2}$.

RESULTS AND DISCUSSION

The hydrothermal reactions of Rb_2CO_3 and I_2O_5 under different Rb:I molar ratios afforded two new rubidium iodates, namely, β-$RbIO_3(HIO_3)_2$ (**1**) and $Rb_3(IO_3)_3(I_2O_5)(HIO_3)_4(H_2O)$ (**2**). Compound **2** crystallizes in the centric space group $P2_1/c$, while compound **1** crystallizes in the acentric polar space group $P1$. α-$RbIO_3(HIO_3)_2$ was structurally characterized in 1980; it crystallized in the centric space group $P\bar{1}$ with cell parameters of a = 8.250(5) Å, b = 8.238(5) Å, c = 8.210(5) Å, α = 108.55(6)°, β = 120.16(7)°, γ = 94.49(6)°, V = 437.66 Å^2, and Z = 2,[26b] which are different from those of our **1**. It is interesting that **1** exhibits a moderate SHG response with a wide optical window.

Table 2. Selected Bond Lengths (Å) for the Two Compounds[a]

β-$RbIO_3(HIO_3)_2$ (**1**)			
Rb(1)−O(15)$^{\#1}$	2.953(9)	Rb(2)−O(11)$^{\#5}$	2.870(9)
Rb(1)−O(1)	3.026(9)	Rb(2)−O(6)	3.000(10)
Rb(1)−O(8)$^{\#2}$	3.047(8)	Rb(2)−O(13)$^{\#6}$	3.009(8)
Rb(1)−O(9)$^{\#2}$	3.066(7)	Rb(2)−O(5)$^{\#3}$	3.050(8)
Rb(1)−O(12)$^{\#2}$	3.118(8)	Rb(2)−O(18)$^{\#6}$	3.067(7)
Rb(1)−O(7)	3.118(7)	Rb(2)−O(17)$^{\#6}$	3.088(8)
Rb(1)−O(5)$^{\#3}$	3.139(8)	Rb(2)−O(16)	3.168(7)
Rb(1)−O(16)	3.153(8)	Rb(2)−O(7)	3.197(8)
Rb(1)−O(3)$^{\#4}$	3.169(8)	Rb(2)−O(3)$^{\#4}$	3.284(9)
Rb(1)−O2	3.408(8)	Rb(2)−O(4)	3.478(8)
I(1)−O(1)	1.808(8)	I(4)−O(10)	1.782(8)
I(1)−O(2)	1.811(8)	I(4)−O(11)	1.809(7)
I(1)−O(3)	1.814(8)	I(4)−O(12)	1.913(6)
I(2)−O(4)	1.807(7)	I(5)−O(13)	1.780(7)
I(2)−O(5)	1.811(7)	I(5)−O(14)	1.796(8)
I(2)−O(6)	1.820(8)	I(5)−O(15)	1.885(7)
I(3)−O(7)	1.781(8)	I(6)−O(16)	1.789(8)
I(3)−O(8)	1.827(7)	I(6)−O(17)	1.790(7)
I(3)−O(9)	1.927(8)	I(6)−O(18)	1.891(8)
$Rb_3(IO_3)_3(I_2O_5)(HIO_3)_4(H_2O)$ (**2**)			
Rb(1)−O(12)	2.883(4)	Rb(2)−O(20)	3.133(4)
Rb(1)−O(21)$^{\#1}$	2.898(5)	Rb(2)−O(8)	3.314(5)
Rb(1)−O(7)$^{\#2}$	2.966(4)	Rb(2)−O(4)$^{\#7}$	3.320(4)
Rb(1)−O(4)$^{\#3}$	2.987(4)	Rb(2)−O(16)	3.456(4)
Rb(1)-O(1W)	2.987(4)	Rb(3)−O(13)$^{\#8}$	2.854(5)
Rb(1)−O(14)	3.042(4)	Rb(3)−O(13)	2.949(4)
Rb(1)−O(15)$^{\#2}$	3.081(4)	Rb(3)−O(10)	2.952(4)
Rb(1)−O(25)	3.125(4)	Rb(3)−O(3)$^{\#9}$	3.007(4)
Rb(1)−O(22)	3.417(4)	Rb(3)−O(26)$^{\#9}$	3.069(4)
Rb(2)−O(1)	2.911(4)	Rb(3)−O(23)	3.094(4)
Rb(2)−O(17)$^{\#4}$	2.950(4)	Rb(3)−O(18)	3.155(4)
Rb(2)−O(15)$^{\#5}$	2.966(5)	Rb(3)−O(16)	3.156(4)
Rb(2)−O(9)	3.025(4)	Rb(3)−O(22)$^{\#9}$	3.194(4)
Rb(2)−O(21)	3.071(4)	Rb(3)−O(17)	3.438(5)
Rb(2)−O(14)$^{\#6}$	3.114(4)	I(5)−O(14)	1.780(4)
I(1)−O(1)	1.795(4)	I(5)−O(12)	1.946(4)
I(1)−O(2)	1.812(4)	I(6)−O(15)	1.777(4)
I(1)−O(3)	1.826(4)	I(6)−O(16)	1.813(4)
I(2)−O(4)	1.774(4)	I(6)−O(17)	1.914(4)
I(2)−O(5)	1.819(4)	I(7)−O(18)	1.795(4)
I(2)−O(6)	1.873(4)	I(7)−O(19)	1.799(4)
I(3)−O(7)	1.794(4)	I(7)−O(20)	1.921(4)
I(3)−O(8)	1.807(4)	I(8)−O(21)	1.767(4)
I(3)−O(9)	1.830(4)	I(8)−O(22)	1.807(4)
I(4)−O(10)	1.788(4)	I(8)−O(23)	1.913(4)
I(4)−O(11)	1.793(4)	I(9)−O(24)	1.790(4)
I(4)−O(12)	1.990(4)	I(9)−O(25)	1.794(4)
I(5)−O(13)	1.774(4)	I(9)−O(26)	1.915(4)

[a] Symmetry transformations used to generate equivalent atoms. For compound **1**: #1, $x, y, z-1$; #2, $x, y+1, z$; #3, $x-1, y, z$; #4, $x+1, y, z$; #5, $x, y, z+1$; #6, $x, y-1, z$. For compound **2**: #1, $-x+1, -y+1, -z+1$; #2, $x, y, z+1$; #3, $x, -y+1/2, z+1/2$; #4, $x-1, y, z$; #5, $-x+1, -y+1, -z$; #6, $x-1, y, z-1$; #7, $x-1, -y+1/2, z-1/2$; #8, $-x+2, -y+1, -z+1$; #9, $x+1, y, z$.

Synthesis. Through hydrothermal reactions of the same starting material of Rb_2CO_3 and I_2O_5 in water, compounds **1**

dx.doi.org/10.1021/ic4028942 | Inorg. Chem. 2014, 53, 1756−1763

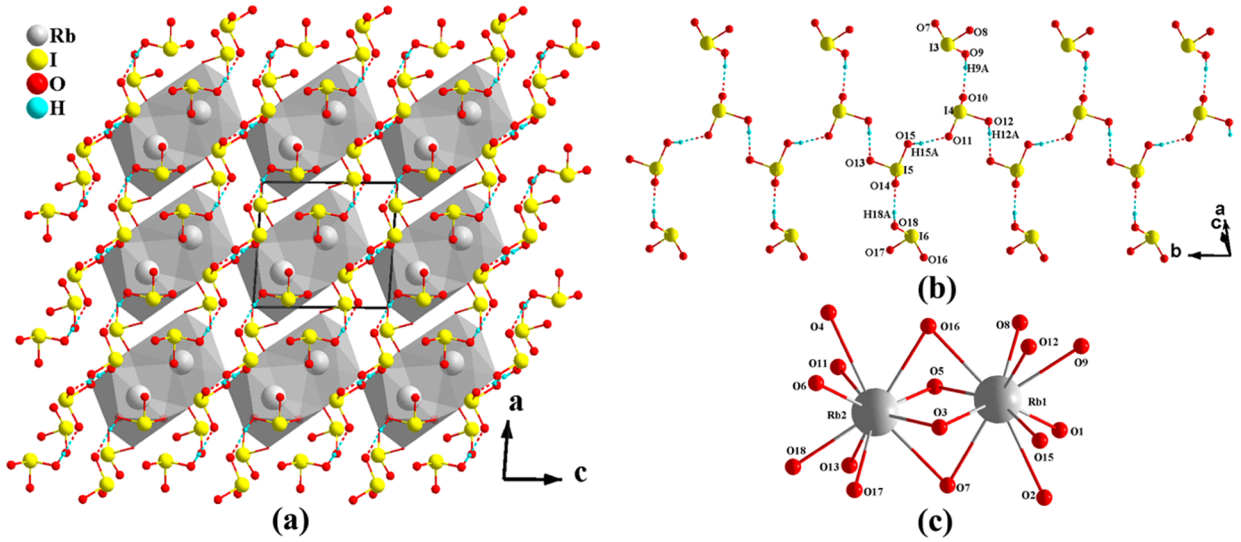

Figure 2. View of the structure of **1** down the *b* axis (a), the 1D $[HIO_3]_n$ chain along the *b* axis (b), and the 0D Rb_2O_{16} unit (c). The hydrogen bonds are drawn as dashed lines, and Rb_2O_{16} dimers are shaded in gray.

and **2**, as well as α-$RbIO_3(HIO_3)_2$ and $Rb_2(I_3O_8)(IO_3)(HIO_3)_2(H_2O)$ which were reported previously, can be synthesized as single phases. The optimized reaction conditions for the single phases of **1** and **2** are described in the Experimental Section, and the reaction conditions for α-$RbIO_3(HIO_3)_2$ and $Rb_2(I_3O_8)(IO_3)(HIO_3)_2(H_2O)$ are listed in Table S1 in the Supporting Information. These four compounds have the same Rb:I ratio, and their structural formulas are very sensitive to the reaction conditions. On the basis of our experiments, when the I_2O_5:Rb_2CO_3 molar ratio employed is lower than 3:1, $RbIO_3$ will be isolated. If the I_2O_5:Rb_2CO_3 molar ratio is higher than 3:1, compounds **1** and **2**, α-$RbIO_3(HIO_3)_2$, and $Rb_2(I_3O_8)(IO_3)(HIO_3)_2(H_2O)$ can be obtained as single phases under very narrow reaction conditions, which indicates that the composition of the final product can be easily affected by the reaction temperature, the Rb_2CO_3:I_2O_5 molar ratio, and the amount of water employed. We noted that a higher reaction temperature is necessary for the preparation of **1**; otherwise, α-$RbIO_3(HIO_3)_2$ will also be formed as an impurity along with **1**. For the synthesis of **2**, a larger amount of Rb_2CO_3 employed may result in the formation of three other compounds instead of **2**. It is also found that a lower cooling rate can improve the crystal qualities of the products and favor the isolation of the single phases.

Structural Description. Compound **1** crystallizes in the noncentrosymmetric triclinic space group *P*1. The structure of **1** is composed of IO_3^- anions and neutral HIO_3 molecules which are interconnected by Rb^+ cations into a 3D structure (Figure 2). Its asymmetric unit consists of two rubidium ions, two IO_3^- anions (containing I(1) and I(2)), and four HIO_3 molecules (containing I(3), I(4), I(5), and I(6)). The IO_3^- anions exhibit three normal I−O bonds ranging from 1.807(7) to 1.820(8) Å, whereas the HIO_3 molecules show two normal I−O bonds (1.780(7)−1.827(7) Å) and one elongated I−OH bond (1.885(7)−1.927(8) Å). These bond lengths are comparable to those previously reported in ternary rubidium iodates.[26] Both Rb^+ cations are ten-coordinated by six IO_3 groups in a unidentate fashion and two IO_3 groups in a bidentate fashion (Figure S3, Supporting Information). The Rb−O distances fall in the range of 2.953(9)−3.408(8) Å for Rb(1) and 2.870(9)−3.478(8) Å for Rb(2). The bond valence sum (BVS) calculations gave values of 5.01, 4.98, 4.62, 4.74, 4.92, and 4.88 for I(1), I(2), I(3), I(4), I(5), and I(6) and 1.02 and 1.06 for Rb(1) and Rb(2), respectively, which are consistent with their expected valences (Table S2, Supporting Information).[34]

$I(1)O_3$, $I(2)O_3$, $HI(3)O_3$, and $HI(6)O_3$ are tetradentate, and each connects with three Rb^+ cations. Two oxygen atoms form a bidentate chelation with a Rb^+ cation, whereas the third one is bidentate and bridges with two metal centers. $HI(4)O_3$ and $HI(5)O_3$ each connects with two Rb^+ cations by using its two oxygen atoms, whereas the third oxygen atom remains noncoordinated (Figure S4, Supporting Information).

A pair of $Rb(1)O_{10}$ and $Rb(2)O_{10}$ polyhedra form a 0D Rb_2O_{16} dimer by sharing four oxygen atoms (O(3), O(7), O(5), O(16)) (Figure 2c). Each Rb_2O_{16} dimer is surrounded by twelve IO_3 or/and HIO_3 groups (containing two I(1), two I(2), two I(3), two I(4), two I(5), and two I(6) atoms). Such Rb_2O_{16} dimers are further interconnected by bridging $I(1)O_3$ and $I(2)O_3$ along the *a* axis, $HI(3)O_3$ and $HI(6)O_3$ along the *b* axis, and $HI(4)O_3$ and $HI(5)O_3$ along the [0−11] direction (Figure S5, Supporting Information), resulting in the formation of a complicated 3D network (Figure 2a).

Furthermore, the HIO_3 molecules are interconnected through hydrogen bonds into a branchlike 1D $[HIO_3]_n$ chain along the *b* axis (Figure 2b). $HI(4)O_3$ and $HI(5)O_3$ are interconnected through hydrogen bonds (O(12)−H(12A)···O(13) and O(15)−H(15A)···O(11)) into a 1D chain, whereas $HI(3)O_3$ and $HI(6)O_3$ hang on both sides of the chain through O(9)−H(9A)···O(10) and O18−H(18A)···O(14) hydrogen bonds, respectively. The hydrogen bond distances and angles range from 2.645(9) to 2.777(1) Å and from 167.3(5)° to 177.0(6)°, respectively (Table S3, Supporting Information). Such 1D chains are further interconnected by Rb_2O_{16} dimers into a 3D network (Figure 2a).

The structure of **1** is quite similar to that of the previously reported α-$RbIO_3(HIO_3)_2$.[26b] α-$RbIO_3(HIO_3)_2$ also exhibits isolated IO_3^- anions and neutral HIO_3 molecules that are separated by Rb^+ cations. The Rb^+ cation in α-$RbIO_3(HIO_3)_2$ is also ten-coordinated with six IO_3 groups in a unidentate fashion and two IO_3 groups in a bidentate fashion. There are also some differences between the structures of α-$RbIO_3(HIO_3)_2$ and **1**.

dx.doi.org/10.1021/ic4028942 | *Inorg. Chem.* 2014, 53, 1756−1763

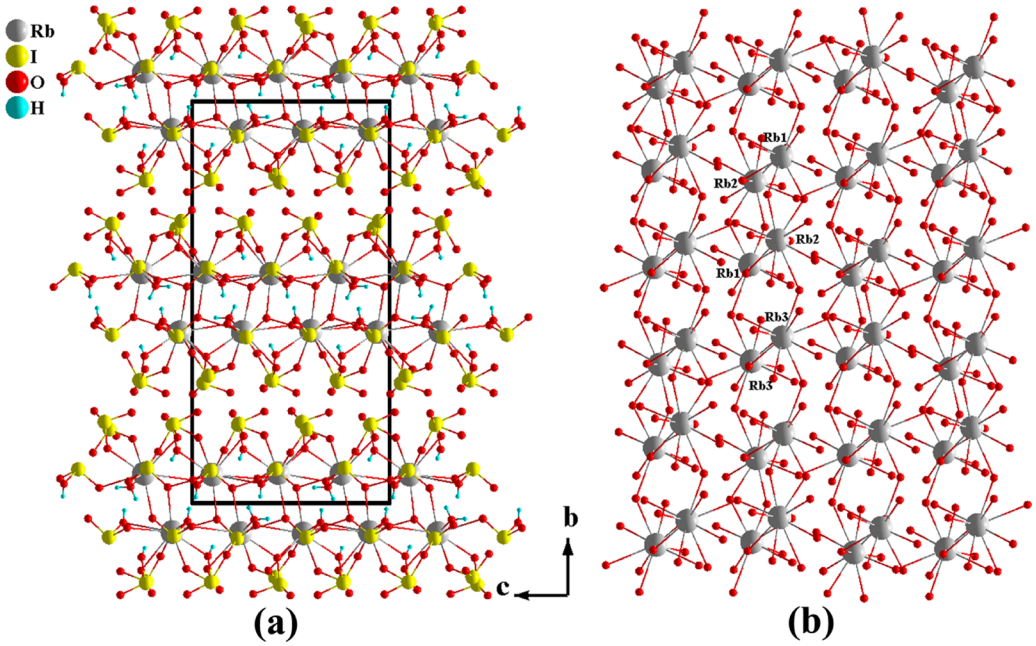

Figure 3. View of the structure of **2** down the *a* axis (a) and the Rb−O layer parallel to the *ac* plane (b).

First, the coordination modes of the IO_3 units are different (Figures S4 and S6a, Supporting Information). In α-$RbIO_3(HIO_3)_2$, $I(1)O_3$ forms a bidentate chelation with a Rb^+ cation and also bridges with a second metal center, $I(2)O_3$ is tetradentate and forms a bidentate chelation with a Rb^+ cation and also bridges with two other metal centers, and $I(3)O_3$ is tridentate and bridges with three Rb^+ cations (Figure S6a, Supporting Information). Second, two RbO_{10} polyhedra form a Rb_2O_{18} dimer via edge-sharing in the α-phase, whereas they form a Rb_2O_{16} dimer through four-vertex-sharing in the β-phase, which results in the different Rb−Rb distances within the dimer (4.873(1) Å for the α-phase and 3.838(2) Å for the β-phase) (Figure 2c; Figure S6b, Supporting Information). Third, the interconnection form of Rb_2O_{16} (or Rb_2O_{18}) dimers and IO_3 groups is different (Figures S5 and S7, Supporting Information). In the α-phase, both $I(1)O_3$ and $I(2)O_3$ bridge with two Rb_2O_{18} dimers and $I(3)O_3$ bridges with three Rb_2O_{18} dimers, whereas in the β-phase each IO_3 unit only bridges with two Rb_2O_{16} dimers. Furthermore, Rb_2O_{18} dimers in the α-phase are bridged by pairs of $I(1)O_3$ groups and pairs of $I(2)O_3$ groups along the *b* axis and *c* axis, respectively, and through pairs of $I(3)O_3$ along the (001) plane (Figure S7, Supporting Information). These different linkage fashions between IO_3 groups and Rb_2O_{16} (or Rb_2O_{18}) dimers resulted in a different 3D network structure for the α-phase (Figure S8, Supporting Information).

Compound **2** crystallizes in the centrosymmetric space group $P2_1/c$. It exhibits a two-dimensional layered structure composed of IO_3^- anions and neutral HIO_3 and dimeric I_2O_5 molecules that are interconnected by Rb^+ cations (Figure 3a). The asymmetric unit contains three Rb^+ cations, three IO_3^- anions, one I_2O_5 molecule, and four HIO_3 molecules. I(1), I(2), and I(3) are in a trigonal IO_3 pyramidal geometry with I−O bond distances ranging from 1.774(4) to 1.873(4) Å. I(4) and I(5) of the I_2O_5 molecule are also coordinated by three oxygen atoms with bond distances of 1.990(4) and 1.946(4) Å for the two bridging I−O bonds and 1.774(4)−1.793(4) Å for the terminal I−O bonds. The HIO_3 molecules exhibit two normal I−O bonds (1.767(4)−1.813(4) Å) and one elongated I−OH bond (1.913(4)−1.921(4) Å). Both $Rb(2)^+$ and $Rb(3)^+$ ions are ten-coordinated with ten oxygen atoms from IO_3, I_2O_5, and HIO_3, whereas the $Rb(1)^+$ ion is nine-coordinated with one oxygen from an aqua ligand and eight oxygen atoms from IO_3 and HIO_3. The Rb−O distances are in the range of 2.883(4)−3.417(4) Å for Rb(1), 2.911(4)−3.456(4) Å for Rb(2), and 2.854(5)−3.438(5) Å for Rb(3). According to the bond valence analyses, Rb and I are in oxidation states of +1 and +5, respectively (Table S2, Supporting Information).[34]

The RbO_x (x = 9 and 10) polyhedra corner- or edge-share into two-dimensional (2D) Rb−O layers parallel to the *ac* plane (Figure 3b). Within the 2D Rb−O layer, two $Rb(3)O_{10}$ polyhedra form a Rb_2O_{18} dimer via edge-sharing, whereas two $Rb(1)O_9$ and two $Rb(2)O_{10}$ polyhedra form a Rb_4O_{30} cluster via edge-sharing. Such Rb_2O_{18} dimers and Rb_4O_{30} clusters are further interconnected alternately via corner-sharing into a 2D Rb−O layer (Figure S9, Supporting Information). The IO_3^- anions and I_2O_5 and HIO_3 molecules cap both sides of the Rb−O layers, resulting in a thicker rubidium iodate layer parallel to the *ac* plane (Figure 3a).

Hydrogen bond interactions are also observed in the structure of **2** (Table S3, Supporting Information). Two $HI(8)O_3$ and two $HI(9)O_3$ molecules form a 0D $[HIO_3]_4$ cluster via hydrogen bonds, whereas $HI(6)O_3$, $HI(7)O_3$, I_2O_5, and H_2O molecules are interconnected through hydrogen bonds into a 0D $[(HIO_3)_2(I_2O_5)(H_2O)]$ cluster (Figure S10, Supporting Information).

It is worthy to compare the structures of the above two compounds with those of $RbIO_3$, α-$RbIO_3(HIO_3)_2$, and $Rb_2(I_3O_8)(IO_3)(HIO_3)_2(H_2O)$ that have been reported previously.[26] All four rubidium hydrogen iodates have the same Rb:I:O:H atom ratio and a higher I:Rb ratio than that of $RbIO_3$. $RbIO_3$ exhibits isolated IO_3^- anions that are separated by Rb^+ cations. For α-$RbIO_3(HIO_3)_2$ and **1**, all IO_3^- anions or HIO_3 molecules are isolated from each other and only interlinked by hydrogen bonds. $Rb_2(I_3O_8)(IO_3)(HIO_3)_2(H_2O)$ exhibits IO_3^- anions, HIO_3 molecules, and trinuclear $I_3O_8^-$ anions. **2** displays

dx.doi.org/10.1021/ic4028942 | *Inorg. Chem.* 2014, 53, 1756−1763

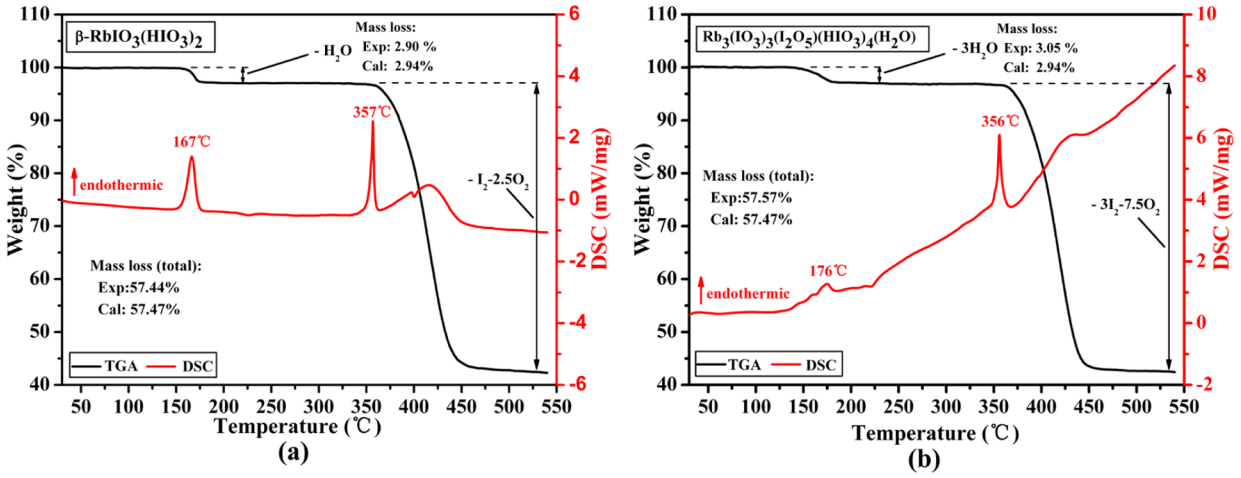

Figure 4. TGA and DSC curves of **1** (a) and **2** (b).

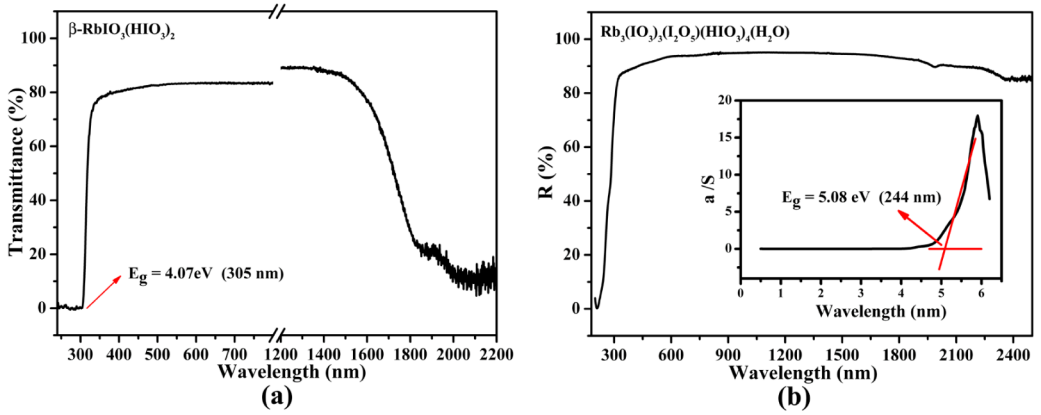

Figure 5. UV−vis−NIR transmittance spectrum of **1** (a) and optical diffuse reflectance spectrum of **2** (b).

IO_3^- anions and dimeric I_2O_5 and HIO_3 molecules. Hence, the I^{5+} cation can form different anions or molecules under different reaction conditions. Furthermore, with the variation of the form of I−O groups, the Rb cations are interconnected into a 3D Rb−O net, a 2D Rb−O layer, and a 0D Rb_2O_n (n = 18 or 16) dimer in $RbIO_3$, $Rb_2(I_3O_8)(IO_3)(HIO_3)_2(H_2O)$ and **2**, and α-$RbIO_3(HIO_3)_2$ and **1**, respectively.

Thermal Stability Studies. TGA studies indicate that both **1** and **2** are thermally stable up to about 150 °C (Figure 4). Then they exhibit two similar steps of weight losses. The small weight losses in the temperature range of 150−180 °C correspond to the release of 1.0 H_2O molecule for **1** and 3.0 H_2O molecules for **2** per formula unit, which are in agreement with the endothermic peaks at 167 °C for **1** and 176 °C for **2** in their DSC diagrams. The observed weight losses of 2.90% for **1** and 3.05% for **2** at 180 °C are very close to their calculated values of 2.94%. The second weight losses in the temperature range of 350−450 °C may be attributed to the release of 1.0 I_2 molecule and 2.5 O_2, 3.0 I_2, and 7.5 O_2 molecule per formula unit for **1** and **2**, respectively. The DSC diagrams of **1** and **2** exhibit strong endothermic peaks at 357 and 356 °C, respectively, which are consistent with their second weight losses. The final residuals for the two compounds at 500 °C were confirmed to be $RbIO_3$ on the basis of a powder XRD study (Figures S2, Supporting Information). The total weight losses of 57.4% for **1** and 57.6% for **2** at 540 °C match well with their calculated values of 57.5%.

Hardness for 1. The Vickers hardness of **1** is measured to be 110 HV, about 2.5 on the Mohs scale, which is comparable to that of the KDP crystal.[35] The result shows that the crystal of **1** can be easily used for machining operation.

Circular Dichroism Spectrum for 1. The solid-state CD spectrum shows a strong peak in the wavelenth range of 300−330 nm (Figure S11, Supporting Information), which is associated with the Cotton effect near the optical band gap. This confirms the optical activity of β-$RbIO_3(HIO_3)$, which is in agreement with its chiral space group $P1$.

Vibrational Spectra for 1 and 2. The IR spectra of the two compounds are very similar, and both exhibit a number of absorption bands: 3447, 1630, 1165, 1095, 819, 775, 738, 640, 613, and 473 cm^{-1} for **1** and 3443, 1627, 1223, 1080, 845, 766, 706, 644, 611, 555, and 457 cm^{-1} for **2** (Figure S12, Supporting Information). The absorption bands in the range of 4000−950 cm^{-1} should be associated with ν_{H-O}. The absorption bands centered at 775, 738, 640, and 613 cm^{-1} for **1** and 766, 706, 644, and 611 cm^{-1} for **2** can be attributed to the symmetric I−O stretching (ν_1). Symmetric I−O bending (ν_2) and asymmetric I−O stretching (ν_3) appeared at 473 and 819 cm^{-1} for **1** and 457 and 555 and 845 cm^{-1} for **2**, respectively. These assignments are in agreement with those previously reported for other related metal iodates.[18−26]

UV−Vis−NIR Spectra for 1 and 2. Figure 5 shows the transmittance spectrum measured by using a 1.5 mm thick slab of **1** (Figure 1c) polished on both sides and the optical diffuse

dx.doi.org/10.1021/ic4028942 | Inorg. Chem. 2014, 53, 1756−1763

reflectance spectrum for **2**. For **1**, the short-wavelength transmission cutoff is located at 305 nm (corresponding to the optical band gap of 4.07 eV), and the IR absorption edge extends to approximately 2100 nm. Furthermore, the crystal exhibits high transparency (above 80%) in the range of 350−1500 nm, implying that there is a wide optical window for optical application.

For **2**, the optical band gap is derived to be 5.08 eV (corresponding to 244 nm) on the basis of its optical diffuse reflectance spectrum using the Kubelka−Munk function.[36] Compared with **1**, the optical band gap of **2** exhibits a large blue shift of about 61 nm. This great blue shift may be associated with their different structures, but its mechanism is still not clear to us so far.

Laser-Induced Damage Threshold for 1. The average energy density of a single pulse for the input laser beam was determined to be 44.94 mJ when the crystal of **1** was broken by the laser (wavelength λ = 1064 nm, pulse duration τ = 10 ns). The $1/e$ radius of the laser spot focused on the crystal was measured to be about 0.28 mm. Hence, the laser-induced damage threshold for **1** is estimated to be about 18.26 J/cm^2. This value is smaller than that for KDP measured at the same wavelength under similar conditions (25−32 J/cm^2),[37] which may be attributed to the lower thermal stability and smaller optical band gap of **1** than those of KDP.[35]

SHG Properties for 1. The SHG signals as a function of particle size from the measurements made on ground and sieved samples of crystals of **1** with a Q-switched Nd:YAG laser of wavelength 1064 nm are shown in Figure 6. For large particle

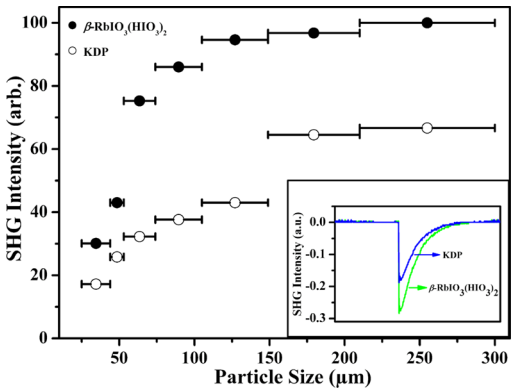

Figure 6. SHG measurements of **1** (●) with KDP (○) as a reference. Oscilloscope traces of the SHG signals for the samples (150−210 μm) of **1** and KDP are shown in the inset.

sizes (150−210 and 210−300 μm), the SHG intensity is nearly independent of the particle size. Features of the curves are very consistent with type I phase-matching behavior according to the rule proposed by Kurtz and Perry.[29] Comparison of the second-harmonic signal produced by sample of **1** and KDP samples in the same particle range of 150−210 μm reveals that **1** exhibits an SHG response about 1.5 times that of KDP. We also measured the SHG responses for **1** using a 2.05 μm Q-switched laser as the fundamental frequency light with the sieved sample; unfortunately, no SHG signal was detected, which may be attributed to the low transmittance in the wavelength of 2.05 μm caused by the lattice water in the structure.

Dipole Moment Analysis. To better understand the arrangement of the asymmetric coordination IO_3^- and HIO_3 units, and the origin of the SHG efficiency, the local and net dipole moments of IO_3^- or HIO_3 units in both compounds were calculated (Table S4, Supporting Information). The lone pair is given a charge of −2 and is localized 1.23 Å away from the I^{5+} cations.[38] The local dipole moments of IO_3 and HIO_3 were calculated to be 14.55−15.89 D for **1** and 13.67−15.43 D for **2**, which are consistent with the previously reported values.[17,20] For **2**, each unit cell contains four asymmetric units and each asymmetric unit contains nine unique I atoms. The *x*-, *y*-, and *z*-components of the polarizations from the four IO_3 units within a unit cell canceled out completely due to the centrosymmetric space group adopted, and the net dipole moment for a unit cell is 0 D. For **1**, the *x*-, *y*-, and *z*-components of the total dipole moment for all the IO_3 units within a unit cell are calculated to be −1.01, −4.26, and −0.82 D, respectively, and the net dipole moment is 4.45 D for the unit cell, which is responsible for the moderate SHG signal observed.

CONCLUSIONS

In summary, two new iodate compounds, namely, polar β-$RbIO_3(HIO_3)_2$ (**1**) and centrosymmetric $Rb_3(IO_3)_3(I_2O_5)(HIO_3)_4(H_2O)$ (**2**), have been synthesized and structurally characterized. For **1**, bulk crystals with dimensions of several millimeters have been obtained by hydrothermal reactions. Linear optical and NLO characterizations demonstrate that **1** exhibits high transparency (above 80%) in the range of 350−1500 nm with a short-wavelength absorption edge of 305 nm, and it is a type I phase-matchable material with an SHG response about 1.5 times that of KDP. Our further research efforts will be devoted to the explorations of other new ternary metal iodates.

ASSOCIATED CONTENT

Supporting Information

X-ray crystallographic files in CIF format, simulated and experimental powder XRD patterns, IR spectra, and calculated bond valence sum. This material is available free of charge via the Internet at http://pubs.acs.org.

AUTHOR INFORMATION

Corresponding Author

*E-mail: mjg@fjirsm.ac.cn. Fax: (+86)591-83704836.

Notes

The authors declare no competing financial interest.

ACKNOWLEDGMENTS

This work was supported by the National Natural Science Foundation of China (Grants 21231006, 21003127, and 21203197).

REFERENCES

(1) Chen, C.; Liu, G. *Annu. Rev. Mater. Sci.* **1986**, *16*, 203−243.
(2) Dunn, M. H.; Ebrahimzadeh, M. *Science* **1999**, *286*, 1513−1517.
(3) Becker, P. *Adv. Mater.* **1998**, *10*, 979−992.
(4) Hallasyamani, P. S.; Poeppelmeier, K. R. *Chem. Mater.* **1998**, *10*, 2753−2769.
(5) (a) Chen, C. T.; Wang, Y. B.; Wu, B. C.; Wu, K. C.; Zeng, W. L.; Yu, L. H. *Nature* **1995**, *373*, 322−324. (b) Wang, S. C.; Ye, N.; Li, W.; Zhao, D. *J. Am. Chem. Soc.* **2010**, *132*, 8779−8786. (c) Wang, S. C.; Ye, N. *J. Am. Chem. Soc.* **2011**, *133*, 11458−11461. (d) Wang, S. C.; Ye, N. *Solid State Sci.* **2007**, *9*, 713−717.

(6) Ye, N.; Chen, Q.; Wu, B. C.; Chen, C. T. *J. Appl. Phys.* **1998**, *84*, 555−558.
(7) Hu, C. L.; Mao, J. G. *J. Phys.: Condens. Matter* **2010**, *22*, 155801.
(8) (a) Sun, C. F.; Yang, B. P.; Mao, J. G. *Sci. China: Chem.* **2011**, *54*, 911−922. (b) Kong, F.; Sun, C. F.; Yang, B. P.; Mao, J. G. *Struct. Bonding (Berlin, Ger.)* **2012**, *144*, 43−104.
(9) Ok, K. M.; Halasyamani, P. S. *Angew. Chem., Int. Ed.* **2004**, *43*, 5489−5491.
(10) Phanon, D.; Gautier-Luneau, I. *Angew. Chem., Int. Ed.* **2007**, *46*, 8488−8491.
(11) Phanon, D.; Mosset, A.; Gautier-Luneau, I. *J. Mater. Chem.* **2007**, *17*, 1123−1130.
(12) Lee, D. W.; Kim, S. B.; Ok, K. M. *Dalton Trans.* **2012**, *41*, 8348−8353.
(13) Liu, X. M.; Li, G. H.; Hu, Y. W.; Yang, M.; Kong, X. G.; Shi, Z.; Feng, S. H. *Cryst. Growth Des.* **2008**, *8*, 2453−2457.
(14) Li, P. X.; Hu, C. L.; Xu, X.; Wang, R. Y.; Sun, C. F.; Mao, J. G. *Inorg. Chem.* **2010**, *49*, 4599−4605.
(15) Kumar, S. M. R.; Melikechi, N.; Selvakumar, S.; Sagayaraj, P. *J. Cryst. Growth* **2009**, *311*, 337−341.
(16) (a) Jerphagnon, H. *Appl. Phys. Lett.* **1970**, *16*, 298−299. (b) Otaguro, W. S.; Wiener-Avnear, E.; Porto, S. P. S. *Appl. Phys. Lett.* **1971**, *18*, 499−501. (c) Dmitriev, V. G.; Konvisar, P. G.; Mikhailov, V. Yu. *Sov. J. Quantum Electron.* **1986**, *16*, 699−701.
(17) (a) Sykora, R. E.; Ok, K. M.; Halasyamani, P. S.; Albrecht-Schmitt, T. E. *J. Am. Chem. Soc.* **2002**, *124*, 1951−1957. (b) Sykora, R. E.; Ok, K. M.; Halasyamani, P. S.; Wells, D. M.; Albrecht-Schmitt, T. E. *Chem. Mater.* **2002**, *14*, 2741−2749. (c) Shehee, T. C.; Sykora, R. E.; Ok, K. M.; Halasyamani, P. S.; Albrecht-Schmitt, T. E. *Inorg. Chem.* **2003**, *42*, 457−462.
(18) (a) Chang, H. Y.; Kim, S. H.; Halasyamani, P. S.; Ok, K. M. *J. Am. Chem. Soc.* **2009**, *131*, 2426−2427. (b) Chang, H. Y.; Kim, S. H.; Ok, K. M.; Halasyamani, P. S. *J. Am. Chem. Soc.* **2009**, *131*, 6865−6873. (c) Ok, K. M.; Halasyamani, P. S. *Inorg. Chem.* **2005**, *44*, 2263−2271.
(19) Suffren, Y.; Gautier-Luneau, I. *Eur. J. Inorg. Chem.* **2012**, *27*, 4264−4267.
(20) (a) Sun, C. F.; Hu, C. L.; Xu, X.; Ling, J. B.; Hu, T.; Kong, F.; Long, X. F.; Mao, J. G. *J. Am. Chem. Soc.* **2009**, *131*, 9486−9487. (b) Sun, C. F.; Hu, C. L.; Xu, X.; Yang, B. P.; Mao, J. G. *J. Am. Chem. Soc.* **2011**, *133*, 5561−5572. (c) Yang, B. P.; Hu, C. L.; Xu, X.; Sun, C. F.; Zhang, J. H.; Mao, J. G. *Chem. Mater.* **2010**, *22*, 1545−1550. (d) Yang, B. P.; Hu, C. L.; Xu, X.; Huang, C.; Mao, J. G. *Inorg. Chem.* **2013**, *52*, 5378−5384. (e) Huang, C.; Hu, C. L.; Xu, X.; Yang, B. P.; Mao, J. G. *Dalton. Trans.* **2013**, *42*, 7051−7058. (f) Sun, C. F.; Hu, C. L.; Kong, F.; Yang, B. P.; Mao, J. G. *Dalton. Trans.* **2010**, *39*, 1473−1479. (g) Sun, C. F.; Hu, T.; Xu, X.; Mao, J. G. *Dalton. Trans.* **2010**, *39*, 7960−7967.
(21) (a) Chen, X. A.; Chang, X. A; Zang, H. G.; Wang, Q.; Xiao, W. Q. *J. Alloys Compd.* **2005**, *396*, 255−259. (b) Chen, X. A.; Zhang, L.; Chang, X. A.; Zang, H. G.; Xiao, W. Q. *Acta Crystallogr.* **2006**, *C62*, i76−i78. (c) Chen, X. A.; Zhang, L.; Chang, X. A; Xue, H. P.; Zang, H. G.; Xiao, W. Q.; Song, X. M.; Yan, H. *J. Alloys Compd.* **2007**, *428*, 54−58.
(22) Nguyen, S. D.; Yeon, J.; Kim, S. H.; Halasyamani, P. S. *J. Am. Chem. Soc.* **2011**, *133*, 12422−12425.
(23) Cao, Z. B.; Yue, Y. C.; Yao, J. Y.; Lin, Z. S.; He, R.; Hu, Z. G. *Inorg. Chem.* **2011**, *50*, 12818−12822.
(24) (a) Hu, T.; Qin, L.; Kong, F.; Zhou, Y.; Mao, J. G. *Inorg. Chem.* **2009**, *48*, 2193−2199. (b) Sun, C. F.; Hu, C. L.; Mao, J. G. *Chem. Commun.* **2012**, *48*, 4220−4222.
(25) (a) Sun, C. F.; Hu, C. L.; Xu, X.; Mao, J. G. *Inorg. Chem.* **2010**, *49*, 9581−9589. (b) Huang, C.; Hu, C. L.; Xu, X.; Yang, B. P.; Mao, J. G. *Inorg. Chem.* **2013**, *52*, 11551−11562. (c) Ling, J.; Albrecht-Schmitt, T. E. *Eur. J. Inorg. Chem.* **2007**, *5*, 652−655. (d) Hector, A. L.; Levason, W.; Webster, M. *Inorg. Chim. Acta* **2003**, *343*, 90−94.
(26) (a) Alock, N. W. *Acta Crystallogr.* **1972**, *B28*, 2783−2788. (b) Soldatov, E. A.; Ilyukhin, V. V.; Kuz'min, E. A.; Belov, N. V. *Dokl. Akad. Nauk SSSR* **1980**, *252*, 615−618. (c) Ok, K. M.; Halasyamani, P. S. *Inorg. Chem.* **2005**, *44*, 9353−9359. (d) Gautier-Luneau, I.; Suffren, Y.; Jamet, H.; Pilmé, J. *Z. Anorg. Allg. Chem.* **2010**, *636*, 1368−1379.
(27) Sykora, R. E.; Mcdaniel, S. M.; Wells, D. M.; Albrecht-Schmitt, T. E. *Inorg. Chem.* **2002**, *41*, 5126−5132.
(28) Shehee, T. C.; Pehler, S. F.; Albrecht-Schmitt, T. E. *J. Alloys Compd.* **2005**, *388*, 225−229.
(29) Kutz, S. K.; Perry, T. T. *J. Appl. Phys.* **1968**, *39*, 3798−3813.
(30) (a) Blessing, R. H. *Acta Crystallogr.* **1995**, *A51*, 33−38. (b) Busing, W. R.; Levy, H. A. *Acta Crystallogr.* **1957**, *A10*, 180−182.
(31) Sheldrick, G. M. *SHELXTL Crystallographic Software Package*, version 5.1; Bruker-AXS: Madison, WI, 1998.
(32) Spek, A. L. *J. Appl. Crystallogr.* **2003**, *36*, 7−13.
(33) (a) Flack, H. D. *Acta Crystallogr.* **1983**, *A39*, 876−881. (b) Flack, H. D.; Bernardinelli, G. *Chirality* **2008**, *20*, 681−690.
(34) (a) Brown, I. D.; Altermatt, D. *Acta Crystallogr.* **1985**, *B41*, 244−247. (b) Brese, N. E.; O'Keeffe, M. *Acta Crystallogr.* **1991**, *B47*, 192−197.
(35) Dmitriev, V. G.; Gurzadyan, G. G.; Nikogosyan, D. N. *Handbook of Nonlinear Optical Crystals*, 3rd ed.; Springer: Berlin, 1999.
(36) Wendlandt, W. M.; Hecht, H. G. *Reflectance Spectroscopy*; Interscience: New York, 1966.
(37) Pritula, I.; Kosinova, A.; Kolybayeva, M.; Puzikov, V.; Bondarenko, S.; Tkachenko, V.; Tsurikov, V.; Fesenko, O. *Mater. Res. Bull.* **2008**, *43*, 2778−2789.
(38) Galy, J.; Meunier, G.; Andersson, S.; Astom, A. *J. Solid State Chem.* **1975**, *13*, 142−159.